Macromolecules

Volume 28, Number 19 September 11, 1995

A Real-Time Simultaneous Small- and Wide-Angle X-ray Scattering Study of *In-Situ* Deformation of Isotropic Polyethylene

Michael F. Butler,[†] Athene M. Donald,*[,†] Wim Bras,[‡,§] Geoffrey R. Mant,[§] Gareth E. Derbyshire,[§] and Anthony J. Ryan[§,⊥]

Cavendish Laboratory, Department of Physics, University of Cambridge, Madingley Road, Cambridge CB3 0HE, U.K., Materials Science Centre, UMIST, Grosvenor Street, Manchester M1 7HS, U.K., Netherlands Organisation for Scientific Research (NWO), The Hague, The Netherlands, and EPSRC Daresbury Laboratory, Daresbury, Warrington, Cheshire WA4 4AD, U.K.

Received March 27, 1995; Revised Manuscript Received June 9, 1995[⊗]

ABSTRACT: Small- and wide-angle X-ray scattering patterns were measured in real time during *in-situ* deformation of isotropic polyethylene at room temperature. A linear low-density polyethylene (LLDPE) was compared with a high-density polyethylene (HDPE) of approximately the same molecular weight. SAXS showed that the start of cavitation in the HDPE coincided with the onset of a stress-induced martensitic transformation detected by WAXS at a low macroscopic strain (~0.06). It is proposed that the transformation mechanism was the $T2_2$ mode. It was found that in the HDPE possible lamellar stack rotation occurred whereas in the LLDPE interlamellar shear was active. Altering the thermal history to change the degree of crystallinity and lamellar population altered the strain at which the martensitic transformation occurred. In the annealed LLDPE a higher crystallinity delayed the onset of the transformation by allowing a greater amount of deformation to occur via other deformation mechanisms. In annealed HDPE, however, the transformation was activated at lower strains since less deformation of the amorphous component was possible.

1. Introduction

In order to characterize deformation of semicrystalline polymers as completely and unambiguously as possible, it is desirable to record data *in situ* during deformation, collecting both small- and wide-angle scattering (SAXS and WAXS, respectively) patterns simultaneously. Although some *in-situ* X-ray work has been performed using conventional X-ray sources,[1-4] most previous work, on isotropic and specially textured samples,[1-3,5,6] has been performed by "post-mortem" analysis, i.e., carrying out the deformation to some predetermined extent at some controlled temperature and subsequently examining the X-ray scattering patterns at room temperature after sample relaxation. Nevertheless, the few studies to date (including this one) utilizing synchrotron radiation, at room temperature[7] and elevated temperatures,[8-10] have demonstrated its feasibility. The use of synchrotron radiation with a combined SAXS/WAXS setup is essential in providing good-quality, unambiguous, information on both the molecular and supramolecular length scales.

Because of its commercial importance, much work has been directed toward understanding the deformation of polyethylene (PE).[5,6] However, the precise details of the molecular and structural changes are still not entirely understood. The main reason for this lies in the complexity of the semicrystalline structure of PE.[11] Bulk isotropic melt-crystallized PE usually crystallizes with a spherulitic morphology,[12] although in commercial grades the spherulites may not possess full spherical symmetry due to rapid cooling. The spherulites are composed of a radial arrangement of chain-folded lamellae.[13,14]

The deformation modes operative in PE involve both the amorphous and the crystalline components.[5,6] Initial deformation is believed to occur via deformation of the amorphous component, involving interlamellar shear, interlamellar separation, and lamellar stack rotation. The deformation resulting from these mechanisms is largely reversible, due to the rubbery nature of the

* To whom correspondence should be addressed.
† Department of Physics, University of Cambridge.
‡ Netherlands Organisation for Scientific Research (NWO).
§ EPSRC Daresbury Laboratory, Daresbury.
⊥ Materials Science Centre, UMIST.
⊗ Abstract published in *Advance ACS Abstracts,* August 1, 1995.

0024-9297/95/2228-6383$09.00/0

amorphous "tie molecules" linking adjacent lamellae.[15,16] Melt-crystallized commercial grade PE contains many of these tie molecules. Any irreversibility will be due to them breaking or being pulled out of the lamellae.[16] Irreversible large-strain plastic deformation results from deformation of the crystalline regions.[1] Processes involved in crystalline deformation are chain slip, in which PE chains slide past each other in the direction of the chain axis (chain slip occurs on the (100)[001] and (010)[001] slip systems[5,6] when the critical resolved shear stress, CRSS, on these systems is reached); transverse slip, in which PE chains slide past each other perpendicular to the chain axis ((100)[010] and (010)-[100] are the most likely transverse slip systems[5,6]); deformation-induced twinning ({110} and {310} twinning have been observed experimentally[5,6,17-19]); and a stress-induced martensitic transformation, in which the orthorhombic structure of undeformed PE is converted to a monoclinic structure.[5,6,18,20-25] The former two crystallographic mechanisms involve large-scale shearing of the structure, whereas the latter two mechanisms involve only an atomic-scale, approximately coherent,[24] shear. Chain slip is proposed to occur in two ways: fine and coarse slip.[5,6] Fine slip involves a small amount of slip on many parallel slip planes, resulting in a divergence of the lamellar normal from the chain axis, whereas coarse slip involves a larger amount of slip on fewer planes, and the lamellar normal and chain axis do not diverge. Many different modes of twinning and martensitic transformation have been proposed,[24] of which only a few are deemed likely to occur on the grounds of strain required to activate them. So far, only two of the four likely martensitic transformation modes have been observed, namely the $T1_1$ and $T2_1$ modes.[5] In this paper we cite evidence for the occurrence of a third mode, the $T2_2$ mode. During the course of deformation a combination of the deformation mechanisms will be operative.

During cold drawing the initial unoriented lamellar state undergoes a transition to a final oriented fibrillar one, in a process known as "necking".[26] Often, during tensile deformation, this is accompanied by a loss of compatibility within the structure and cavitation occurs (noticeable by a distinct whitening of the sample and a dramatic increase in X-ray scattering at small angles due to the voids). The lamellae constituting the unoriented material undergo some or all of the mechanisms mentioned above until they fragment. The fragments form much smaller crystalline blocks from which the dense-packed microfibrils are drawn out. The nature of this process is still unclear; some workers have cited evidence for partial melting during drawing followed by recrystallization in a more oriented state;[27-29] others claim that the deformation is purely crystallographic and involves the nucleation and glide of screw dislocations.[30-32]

It is understood that the mechanical properties depend crucially on a variety of factors, including chain length, branch length and frequency, percentage crystallinity, and crystallite pefection.[33] In this study, in order to compare PE's with different structures, a linear low-density polyethylene (LLDPE) with 4-methyl-1-pentene branches and a high-density polyethylene (HDPE) with negligible branching were studied. Furthermore, by altering the thermal history experienced by different samples, the percentage crystallinity, lamellar population, and lamellar thickness could be altered and the effect of this upon deformation investigated.

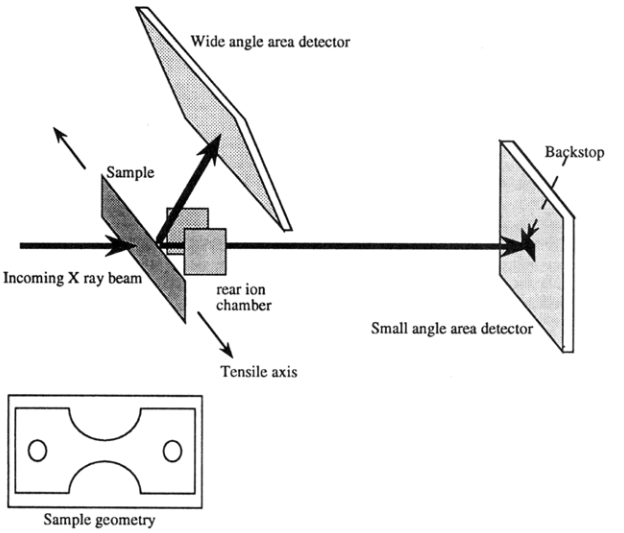

Figure 1. Schematic diagram of the experimental setup, with the sample geometry shown inset.

2. Experimental Section

2.1. Materials and Sample Preparation. The materials used in this study were an HDPE and an LLDPE supplied by BP Chemicals Ltd. The HDPE had a molecular weight M_w = 134 000 with a polydispersity ratio of M_w/M_n = 6.3. The LLDPE had a molecular weight M_w = 126 000, polydispersity ratio M_w/M_n = 4.2, and a 4-methyl-1-pentene comonomer content giving rise to an isobutyl side chain branching of ~21 side chains per 1000 carbon atoms.

Plaques were formed by compression molding the molten PE at 190 °C for 5 min with a load of 20 tons applied. The press was water-cooled, with an initial cooling rate of approximately 50 °C/min, becoming slower as the press cooled. The thicknesses of the HDPE and LLDPE plaques were 0.9 and 1.9 mm, respectively. Specially shaped samples for tensile testing were cut from these plaques. They were 50 mm long and 20 mm wide, with two semicircular cutouts of radius 8 mm to ensure that yielding always occurred in the X-ray beam. The sample geometry is shown in Figure 1 (inset).

Some samples were subjected to annealing treatments to alter the percentage crystallinity, lamellar thickness, and lamellar population. The treated HDPE samples were annealed for 70 min at 132 °C in vacuum. The treated LLDPE samples were annealed for 60 min at 113 °C in vacuum. Samples left to cool slowly (denoted by SC) were left in the oven, in vacuum, until it had reached room temperature. The cooling rate for these samples was approximately 0.5 °C/min until the sample reached about 80 °C, becoming progressively slower to less than 0.1 °C/min by the time the samples had reached room temperature, after several hours. Quenched samples (denoted by Q) were removed after the relevant time at the annealing temperature and plunged into liquid nitrogen. Untreated samples, which had undergone no annealing treatments after manufacture, are denoted by U.

2.2. DSC. Differential scanning calorimetry (DSC) was used to obtain the crystallinity of the samples and information on the lamellar populations and thicknesses. Measurements were taken on a Perkin-Elmer DSC7 equipped with an Intracooler II. Data analysis was performed using Perkin-Elmer 7 Series UNIX software running on a PC. The lamella thickness, L_c, was estimated from the melting point, T_m, by rearranging the equation for the melting point, T_m.[34]

$$T_m = T_{m0}\left(1 - \frac{2\sigma_e}{L_c \Delta h}\right) \tag{1a}$$

$$L_c = \frac{2\sigma_e}{\Delta h}\left(\frac{T_{m0}}{T_{m0} - T_m}\right) \tag{1b}$$

Using the value of (93 ± 8) × 10^{-7} J/cm^2 for the fold surface energy, σ_e,[34] employing 280 J/cm^3 for the heat of fusion of

Table 1. Structural Information Obtained from DSC

sample	L_1, nm	L_2, nm	crystallinity, %	d_1, nm	d_2, nm
HDPE U	32.0 ± 2.8		70.04 ± 0.13	45.7 ± 2.8	
HDPE SC	38.9 ± 3.3		75.56 ± 0.32	51.5 ± 3.3	
HDPE Q	38.0 ± 3.3	16.8 ± 1.4	72.76 ± 0.26	52.2 ± 3.3	23.1 ± 1.4
LLDPE U	16.1 ± 1.4		34.63 ± 0.25	46.5 ± 1.4	
LLDPE SC	14.9 ± 1.3	8.9 ± 0.8	38.20 ± 0.44	39.0 ± 1.3	23.2 ± 0.8
LLDPE Q	16.8 ± 1.4	8.6 ± 0.8	36.58 ± 0.15	45.9 ± 1.4	23.5 ± 0.8

crystal, Δh,[34] and taking the equilibrium melting temperature, T_{m0}, to be equal to 145.8 °C,[34] lamellar thicknesses could be estimated.

The percent crystallinity was calculated from the specific heat of fusion by taking the specific heat of fusion of perfectly crystalline PE to be 293 J/g.[35] A crude estimate for the long period was derived from the percentage crystallinity and the lamellar thickness.

2.3. Load–Extension Curves. Load–extension curves for samples subjected to the same annealing treatments as those deformed in the X-ray beam were obtained independently using a Rheometrics Ltd. Miniature Materials Tester (Minimat) with a 1000 N load beam under PC control. Curves were obtained for HDPE and LLDPE samples drawn at 5.0 mm/min up to extensions of 60 mm.

2.4. Real-Time SAXS/WAXS Measurement during *In-Situ* Deformation. X-ray experiments were performed on station 8.2 at the Synchrotron Radiation Source (SRS) at the Daresbury Laboratory in the United Kingdom. The details of the storage ring, radiation and camera geometry, and data collection electronics have been described elsewhere.[36] The experimental setup is shown schematically in Figure 1 and has been described in more detail by Bras et al.[7] The high-intensity, low-divergence beam had a wavelength approximately that of Cu Kα radiation (λ = 1.52 Å) and was made monochromatic with a bent single crystal. The beam was collimated with slits and had a size of approximately 0.3 × 3.5 mm² in the focal plane, which was situated between the two detectors. With the SRS at 2 GeV and 250 mA the beam intensity is about 4 × 10^{10} photons/s. Two gas-filled proportional wire chambers (area detectors) were used to collect the diffraction pattern. X-rays scattered through small angles were detected by an area detector positioned 3.7 m from the sample. Simultaneously, X-rays scattered through wide angles were detected with another area detector positioned at 45° to the direct beam at a distance of 0.35 m. To eliminate air scattering, a tent, constructed from a light frame covered with Mylar 25 μm thick, filled with helium was positioned between the sample and the wide-angle detector, and a vacuum chamber was positioned between the tent and the small-angle detector.

The samples were deformed in tension at room temperature *in situ* in a Minimat with a 200 N load beam. Extension rates of 0.5 and 5.0 mm/min were used. The maximum strain reached for samples drawn at 0.5 mm/min was 0.625 and for those drawn at 5.0 mm/min was 1.250. Owing to the complicated sample geometry, the strain was calculated approximately using

$$\epsilon = e/l \tag{2}$$

where e was the sample extension and l was the initial gauge length (20 mm). The strain value cannot be regarded as absolute but will be internally consistent. The load could not readily be converted into stress, due to the complicated shape of the sample.

SAXS and WAXS patterns were obtained simultaneously during deformation. The full diffraction circle was not measured for the wide-angle scattering. Data were collected for 20 frames, each frame lasting for 15 s, before being downloaded for storage. The dead time between frames was 10 μs.

To compensate for fluctuations in incident beam intensity, both small- and wide-angle scattering data were normalized with respect to the readings on the ion counters placed in front of and behind the sample. Corrections were made for sample thickness, sample transmission, and detector nonlinearity. The background scattering was subtracted from both SAXS and WAXS data. There was no need to desmear the data due to the point collimated beam size compared with the pixel size of the area detectors. The channel numbers of the small-angle area detector were calibrated using wet rattail collagen.

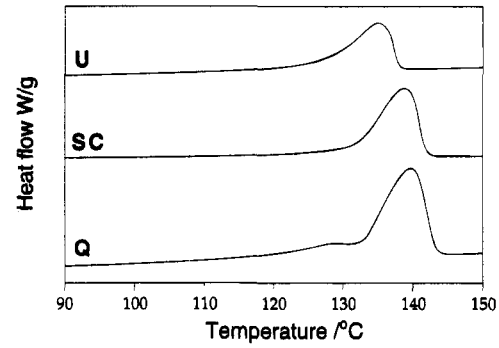

Figure 2. DSC curves showing the melting transition for the untreated (U), slow-cooled (SC), and quenched (Q) HDPE samples.

The Lorentz correction, which corresponds to multiplying the intensity by q^2, where **q** is the scattering vector, was applied to all the SAXS data. The scattering vector is taken to be

$$|\mathbf{q}| = q = \frac{2\pi}{d} \tag{3}$$

where d is the long period. The Lorentz correction is necessary in a randomly oriented sample to correct for the different probabilities of planes being in the reflection condition.[37] In applying this correction, the assumption is made that the morphology is locally lamellar but globally isotropic,[38] i.e., that the lamellae are randomly oriented throughout the whole sample, which is correct for undeformed PE but less so when the structure has become fibrillar.

3. Results

3.1. HDPE. 3.1.1. DSC. DSC curves, showing the melting transition, are shown in Figure 2. The quenched samples have bimodal melting curves, implying that there are two different populations of lamellar thicknesses in the quenched HDPE, whereas untreated and slow-cooled samples have only one melting endotherm, indicating a unimodal lamellar thickness population. Annealing was found to increase the crystallinity. The slow-cooled samples were the most crystalline followed by the quenched and then the untreated samples. Table 1 shows the information derived from the DSC experiments, using eq 1.

3.1.2. WAXS. An example of one of the wide-angle X-ray scattering patterns obtained from a sample before it had experienced much deformation is shown in Figure 3a. The region within the white lines is the equatorial region for which the peak intensities (for all the samples) were measured. The load direction is marked LD and was perpendicular to the X-ray beam. The very intense (110) and (200) reflections from the orthorhombic structure are clearly visible, along with some weaker reflections from other planes. The diffraction patterns were indexed using the unit cell dimensions of orthorhombic PE[39] (a = 7.40 Å, b = 4.93 Å, c = 2.54 Å). The

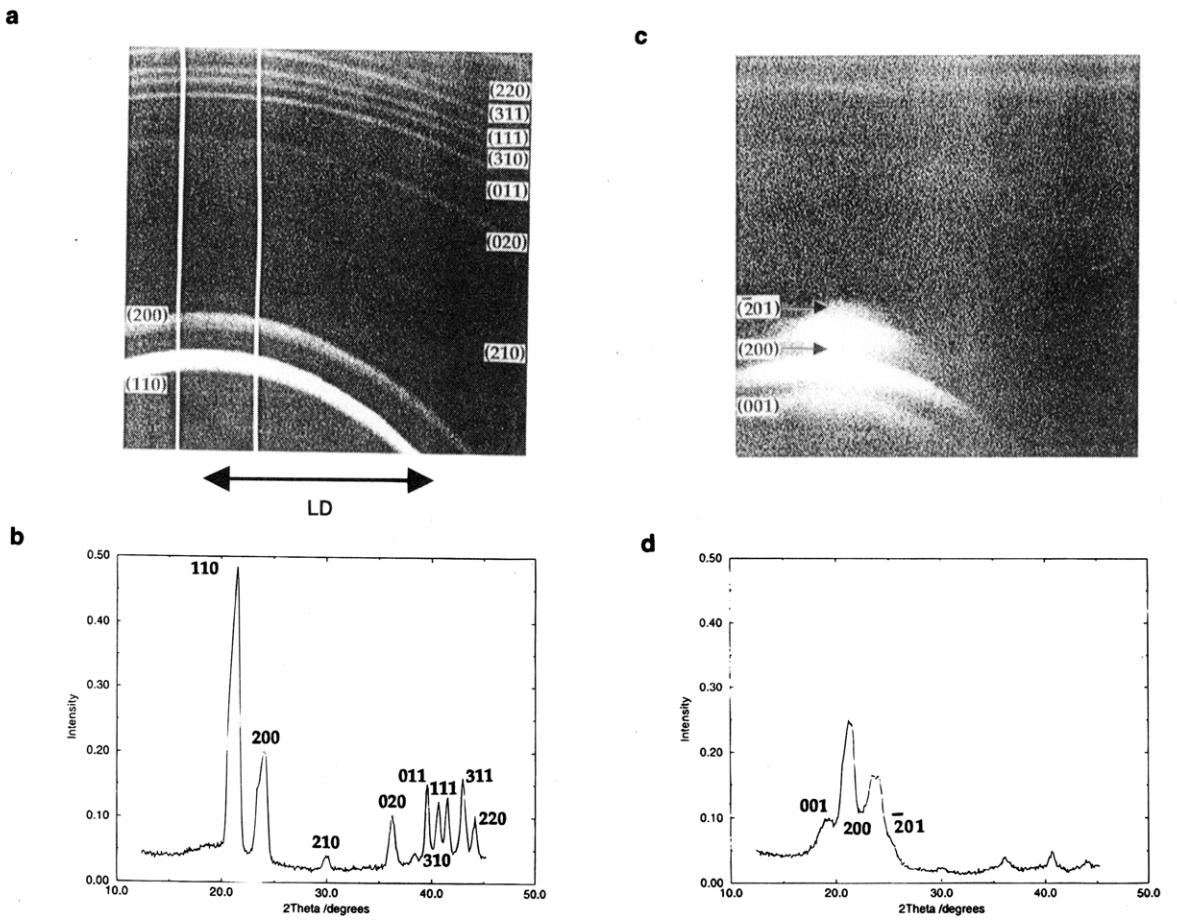

Figure 3. (a) Indexed WAXS pattern for undeformed HDPE. (b) Equatorial peak intensities. (c) Indexed WAXS pattern after 25 mm extension showing indexed monoclinic reflections. (d) Equatorial peak intensities after 25 mm extension (intensity is in arbitrary units).

Table 2. Strains at Which the Monoclinic ($\bar{2}01$) Peak Appeared, ϵ_1, Reached a Constant Intensity, ϵ_2, and Cavitation Began ϵ_{void} (for HDPE)

sample	extension rate, mm/min	ϵ_1	ϵ_2	ϵ_{void}
HDPE U	0.5	0.176 ± 0.003	0.253 ± 0.011	0.179 ± 0.003
	5.0	0.353 ± 0.032	0.417 ± 0.020	0.353 ± 0.032
HDPE SC	0.5		0.230 ± 0.011	
	5.0	0.064 ± 0.032	0.253 ± 0.023	0.064 ± 0.032
HDPE Q	0.5	0.061 ± 0.003	0.115 ± 0.011	0.061 ± 0.032
	5.0	0.064 ± 0.032	0.172 ± 0.023	0.064 ± 0.032
LLDPE U	0.5	0.202 ± 0.007	0.299 ± 0.023	
	5.0	0.160 ± 0.032	0.353 ± 0.023	
LLDPE SC	0.5	0.247 ± 0.007	0.391 ± 0.023	
	5.0	0.224 ± 0.032	0.480 ± 0.023	
LLDPE Q	0.5	0.247 ± 0.007	0.391 ± 0.023	
	5.0	0.224 ± 0.032	0.353 ± 0.023	

intensities of the reflections in the equatorial region are shown in Figure 3b.

During deformation extra reflections appeared at low strains, before the WAXS pattern had become oriented to give a fiber diffraction pattern. Figure 3c shows a WAXS pattern in which these extra reflections are present, with the peak intensities shown in Figure 3d. These new reflections can be identified as arising from the monoclinic phase,[24] indexing as ($\bar{2}01$), (200), and (001) (using a = 8.09 Å, b = 4.79 Å, c = 2.53 Å), indicating that a stress-induced martensitic transformation had occurred.

The strain at which the monoclinic ($\bar{2}01$) reflection first appeared was taken to be the strain at which the martensitic transformation had been activated. It is shown in Table 2, as the value ϵ_1, for all of the samples studied. From Table 2 it is immediately apparent that annealing the HDPE reduced the strain at which the stress-induced martensitic transformation occurred. (It should be noted that in the HDPE slow-cooled sample drawn at 0.5 mm/min, a small amount of monoclinic material was present before the experiment had commenced. This was most probably due to inadvertent deformation of the sample before drawing.)

In Figure 4 the change in monoclinic ($\bar{2}01$) intensity during strain for the untreated and slow-cooled HDPE drawn at 5.0 mm/min is compared. For both untreated and annealed samples, the monoclinic ($\bar{2}01$) reflection increased in intensity until a certain strain was reached, denoted by ϵ_2 in Table 2. In the untreated HDPE it then remained constant, but in the slow-cooled HDPE samples drawn at 5.0 mm/min it decreased as deformation

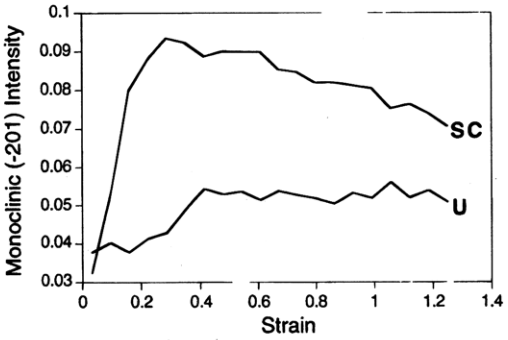

Figure 4. Monoclinic ($\bar{2}01$) intensity (arbitrary units) vs strain for untreated (U) and slow-cooled (SC) HDPE drawn at 5.0 mm/min.

continued. Accompanying the increase in the monoclinic ($\bar{2}01$) intensity was a decrease in the intensity of the orthorhombic (110) peak. The orthorhombic (200) peak intensity remained virtually constant throughout deformation. The reflections at larger scattering angles virtually disappeared. During deformation all of the reflections became less isotropic as the PE chains became increasingly aligned with the tensile axis (LD).

Figures 5a–c show the evolution of the peak intensities with strain for untreated, slow-cooled, and quenched HDPE, respectively, drawn at 5.0 mm/min. Most noticeable is the difference between the untreated and the annealed (slow-cooled and quenched) HDPE. The orthorhombic (110) peak decreased in intensity quite markedly for the annealed samples, but much less so for the untreated sample. The same was found for the HDPE samples drawn at 0.5 mm/min. The increase in intensity, at a strain of approximately 1.0, of the orthorhombic (110) peak in the quenched HDPE drawn at 5.0 mm/min, seen in Figure 5c, was due to relaxation after the sample broke.

The decrease in intensity of the orthorhombic (110) peak was correlated with the increase in intensity of the monoclinic ($\bar{2}01$) peak. This is shown by the straight line in Figure 6, in which the orthorhombic (110) intensity is plotted against the monoclinic ($\bar{2}01$) intensity. Each point corresponds to a different strain. Similar graphs were obtained for the other HDPE (and LLDPE) samples drawn at both extension rates.

Thermal history had an effect on the deformation behavior. Annealed HDPE samples underwent the stress-induced martensitic transformation at lower strains than the untreated samples. For the annealed samples, the strain at which the martensitic transformation was complete was higher for the slow-cooled samples than for the quenched ones. For the untreated samples extension rate was also shown to affect the strain at which the martensitic transformation occurred (shown in Table 2).

3.1.3. SAXS. In all of the HDPE samples cavitation occurred, which led to an increase in SAXS and whitening of the deformed region. The strains at which the voids were formed in the HDPE, ϵ_{void}, taken as the strain at which the small-angle scattered intensity began to increase markedly, are given in Table 2 (note that in the slow-cooled sample drawn at 0.5 mm/min there was an initial void content before the experiment commenced). The values of the martensitic transformation strain are also given. From Table 2 it can be seen that the onset of the stress-induced martensitic transformation coincided with the onset of cavitation. In the annealed HDPE samples drawn at 5.0 mm/min the cavitation ceased to increase after a certain strain was reached.

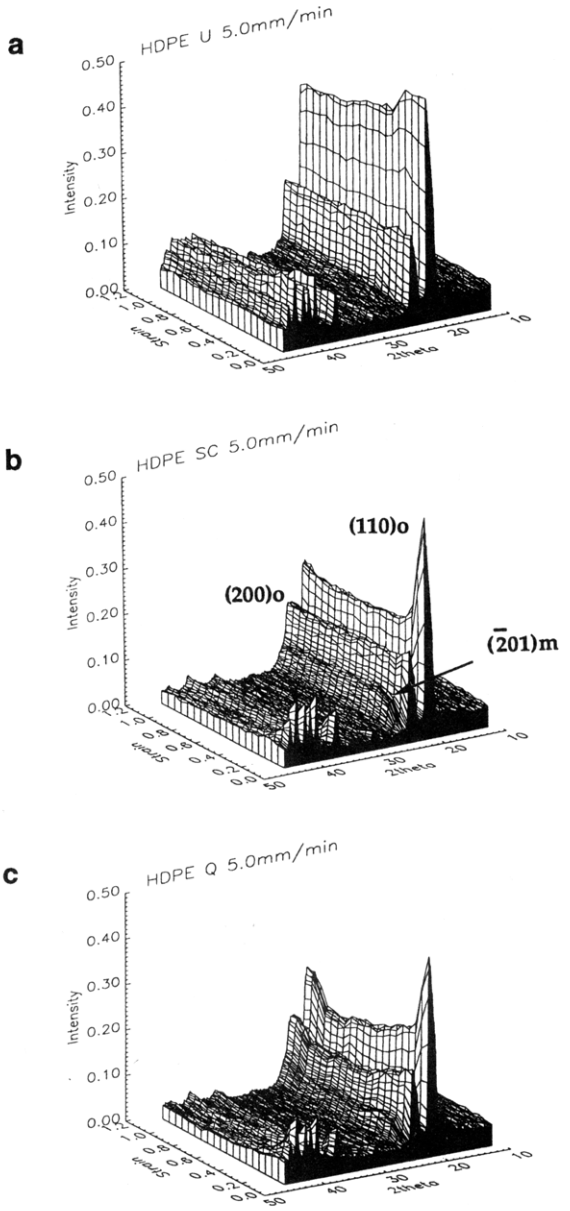

Figure 5. Three-dimensional plot of $I(2\theta)$ vs 2θ vs strain showing the evolution of the wide-angle reflections during drawing for HDPE drawn at 5.0 mm/min: (a) untreated; (b) slow-cooled; (c) quenched. The orthorhombic (110) and (200) and the monoclinic ($\bar{2}01$) reflections are labeled on the slow-cooled HDPE. Intensity is in arbitrary units.

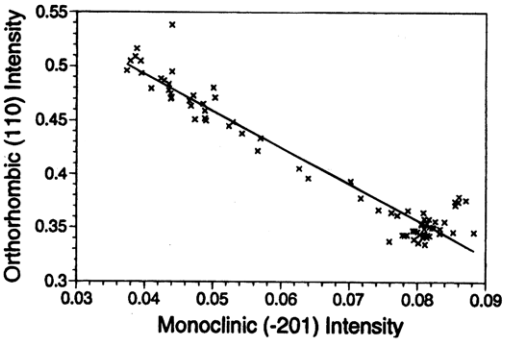

Figure 6. Direct correlation between the decrease in the orthorhombic (110) intensity with the increase in the monoclinic ($\bar{2}01$) intensity (in arbitrary units).

Table 3. SAXS Peak Values, with Corresponding Long Periods, d, and Long Periods Calculated from the DSC Data

	SAXS				DSC	
sample	q_1, $(nm)^{-1}$	q_2, $(nm)^{-1}$	d_1, nm	d_2, nm	d_1, nm	d_2, nm
HDPE U	0.24	0.48	26.2		45.7 ± 2.8	
HDPE SC	0.17	0.34	37.0		51.5 ± 3.3	
HDPE Q	0.17	0.37	37.0	17.0	52.2 ± 3.3	23.1 ± 1.4
LLDPE U	0.26	0.71	24.2	8.9	46.5 ± 1.4	
LLDPE SC	0.25	0.66	25.1	9.5	39.0 ± 1.3	23.2 ± 0.8
LLDPE Q	0.25	0.69	25.1	9.1	45.9 ± 1.4	23.5 ± 0.8

As in the case of the WAXS patterns, the intensity of the scattered X-rays was measured in the equatorial regions of the SAXS patterns, perpendicular to LD. Figure 7a shows the evolution of small-angle scattered uncorrected intensity with q and strain for untreated HDPE drawn at 5.0 mm/min. The peak visible at low strains is attributed to scattering from lamellae, although, as can be seen, it is soon overwhelmed by scattering from the microvoids. Figure 7b shows a similar plot for slow-cooled HDPE drawn at 5.0 mm/min, in which the initial lamellar peak is barely visible due to the rapid increase in void scattering, which can be seen to level out at a constant value.

Figures 8a and 8b show equatorial Lorentz-corrected intensities from undeformed slow-cooled and quenched HDPE, respectively. Two peaks are clearly apparent. In the untreated and slow-cooled HDPE the peak at higher q was found to correspond to the second-order peak of the lamellae spacing. In the quenched HDPE this was not the case, and the higher q peak must have been due to scattering from thinner lamellae. This information agreed qualitatively with the information on the lamellar population given by DSC (shown in Table 3). Samples with a bimodal melting curve exhibited SAXS peaks from two lamellar thicknesses whereas samples with one melting point showed SAXS peaks due to scattering from lamellae of one thickness only.

Figure 9 shows a plot of the long period against strain for the untreated HDPE drawn at 5.0 mm/min. The peaks remained at constant q throughout deformation, implying a constant long period.

3.1.4. Macroscopic Behavior of HDPE. The load–extension curves for the HDPE samples drawn at 5.0 mm/min are shown in Figure 10. The thicker regions of the curves are where the monoclinic phase was detected from the WAXS patterns for the samples deformed *in situ*.

Most noticeable was the marked difference between the HDPE samples with different thermal histories. The untreated HDPE was ductile and formed a stable neck whereas both annealed HDPE samples were much more brittle and the neck fractured. They also had a sharper yield point.

The appearance of the HDPE samples after deformation is shown in Figure 11.

3.2. LLDPE. 3.2.1. DSC. DSC curves obtained from the LLDPE samples are shown in Figure 12. It is immediately apparent from the bimodal melting curves of the slow-cooled and quenched LLDPE that annealing the LLDPE produced a lamellar population with two lamellar thicknesses, L_1 and L_2. The untreated sample contained lamellae of only one thickness. As shown in Table 1, both annealed samples had a higher percentage crystallinity than the untreated LLDPE. Annealing did not, however, alter the lamellar thickness significantly as these are defined by the branch structure.

3.2.2. WAXS. Similar behavior was observed during deformation for the LLDPE as for the HDPE; i.e., reflections from the stress-induced monoclinic phase appeared at low strains. Unlike the HDPE, however, the martensitic transformation occurred at higher strains in the annealed samples than in the untreated sample, for both extension rates (see Table 2). Figure 13 shows the evolution of the equatorial peak intensities for the untreated, slow-cooled, and quenched LLDPE. It can be seen that the behavior of the untreated and annealed LLDPE was much more similar than that of the untreated and annealed HDPE samples. The intensity of the monoclinic ($\bar{2}01$) reflection remained constant after reaching the strain ϵ_2 in Table 2.

3.2.3. SAXS. No cavitation occurred in the LLDPE, and the amount of small-angle scattering decreased as deformation progressed. All of the undeformed LLDPE samples had two small-angle Bragg peaks, similar to those shown in Figure 8 for HDPE. No second orders were detected. The SAXS data again correlated with the DSC data (see Table 3) with the exception of the untreated LLDPE, which DSC predicted to contain lamellae of only one thickness but SAXS predicted to contain two lamellar thicknesses. However, the long periods and lamellar thicknesses are mean values, and an asymmetric long period distribution will shift the second-order SAXS maximum such that $q_2 \neq 2q_1$. This may explain the discrepancy between SAXS and DSC for untreated LLDPE. During deformation the peaks became broader. The peak at higher q became too weak to distinguish after a very small strain.

In Figure 9 the long spacing is plotted for untreated LLDPE. During deformation it shifted to higher q, implying a decrease in the long period. Most of the decrease in long period occurred at the earlier stages of deformation, up to strains of approximately 0.50 (the samples were drawn to a maximum strain of about 1.25).

3.2.4. Macroscopic Behavior of LLDPE. The load–extension curves for the LLDPE samples drawn at 5.0 mm/min are shown in Figure 14, with the thicker portions of the curves corresponding to the regions in which the monoclinic phase was detected in the samples deformed *in situ*. Both annealed and untreated LLDPE were ductile and formed stable necks. They are shown after deformation in Figure 15. The samples physically relaxed substantially, and a twist formed in the neck. The length of the untreated LLDPE decreased from 80 to 64 mm, the slow-cooled LLDPE to 68 mm, and the quenched LLDPE to 66 mm.

4. Discussion

Combination of the X-ray scattering data with the DSC results allows us to propose the deformation mechanisms occurring in the HDPE and LLDPE samples. Although there is a discrepancy between the values of lamellar thickness given by SAXS and DSC (shown in Table 3), DSC remains useful to confirm the structural information given by SAXS. The discrepancy most probably results from the values of the fold surface energy and equilibrium melting point, used in eq 1, being incorrect for the materials we have used. Since the precise values of lamellar thickness are not important here, we draw attention instead to the qualitative information obtained from DSC.

4.1. HDPE. The constant long period in the HDPE during deformation (Figure 9) suggests that the operative deformation mechanism of the amorphous compo-

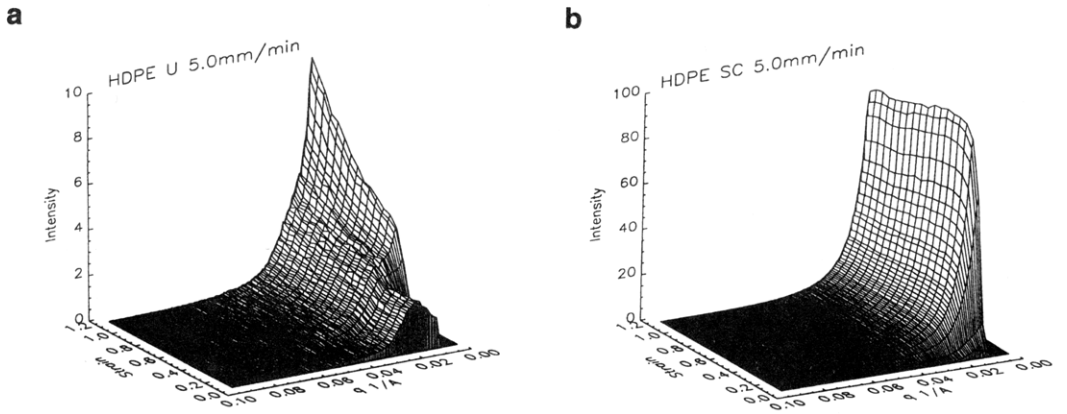

Figure 7. Three-dimensional plot of $I(q)$ vs q vs strain showing the evolution of the small-angle peak for (a) untreated and (b) slow-cooled HDPE drawn at 5.0 mm/min.

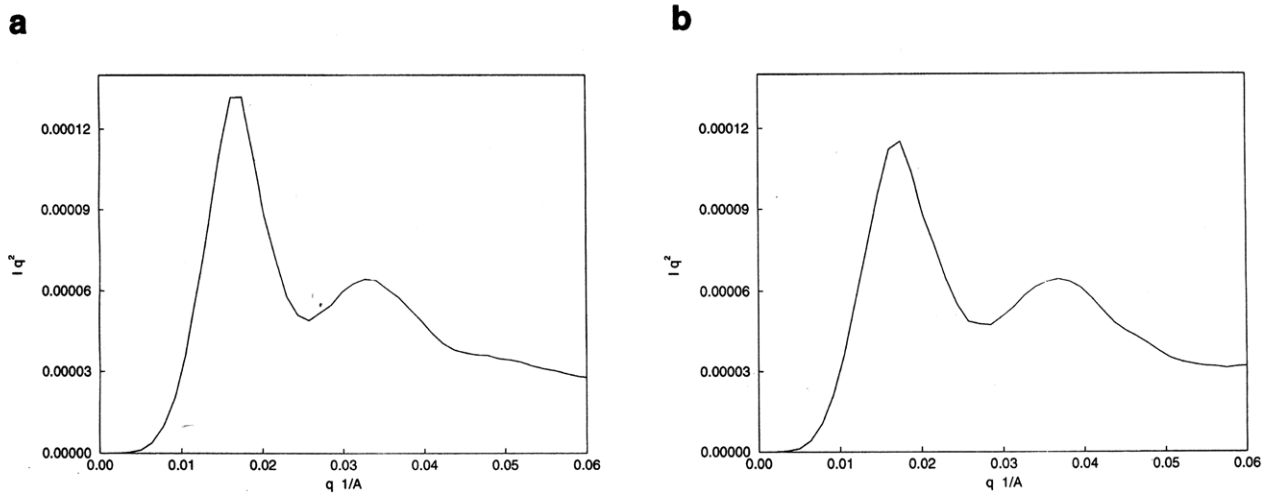

Figure 8. Lorentz-corrected equatorial intensities (arbitrary units) from SAXS for (a) slow-cooled and (b) quenched HDPE, showing the two peaks. In the slow-cooled HDPE the peak at higher q is a second order whereas in the quenched HDPE it is from thinner lamellae.

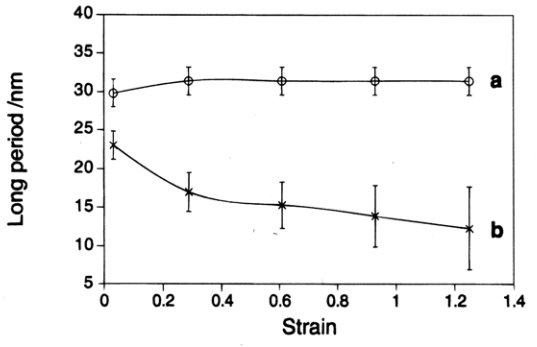

Figure 9. Plot of the long period against strain for (a) untreated HDPE and (b) untreated LLDPE, both drawn at 5.0 mm/min, showing the constant long period during deformation for HDPE and the decrease in long period during deformation for LLDPE.

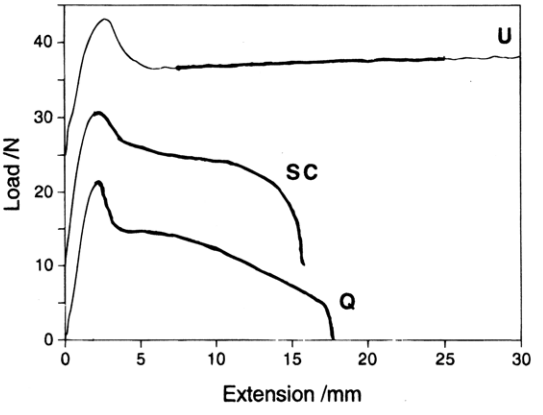

Figure 10. Load–extension curve the untreated (U), slow-cooled (SC), and quenched (Q) HDPE samples drawn at 5.0 mm/min.

nent is lamellar stack rotation (shown in Figure 16)—since this maintains a constant long period spacing. Annealing increases the percentage crystallinity and lamellar thickness (as shown by DSC and SAXS and displayed in Tables 1 and 3). If there is any contribution to the deformation by an amorphous component, this increase in crystallinity must reduce it. Table 2 shows that the strain for the onset of the monoclinic transformation ϵ_1 is decreased by annealing, confirming a reduction in the contribution of the amorphous component. Thus the amorphous phase is playing a role and lamellar stack rotation must be taking place.

Because the martensitic transformation occurred at some finite strain, rather than from the onset of deformation, the transformation must occur after the mechanisms of lamellar deformation involving the amorphous regions and/or crystallographic slip have already been activated, as expected.[5] However, the occurrence of the martensitic transformation at rather low macroscopic strains for some samples (~0.06 for the annealed HDPE samples) suggests that it may be in competition with the other mechanisms at an early stage of deformation. Indeed, it has been found, albeit

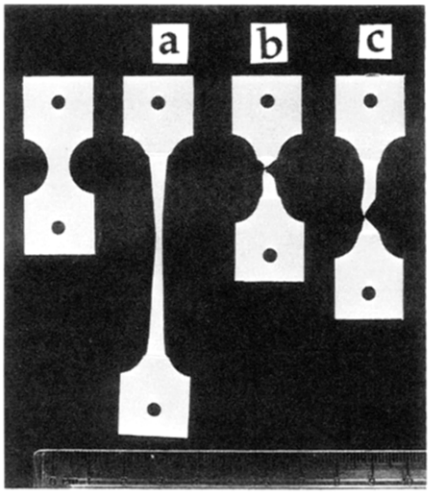

Figure 11. Appearance of the HDPE samples: (a) untreated; (b) slow-cooled; (c) quenched. The unlabeled sample is an undeformed specimen.

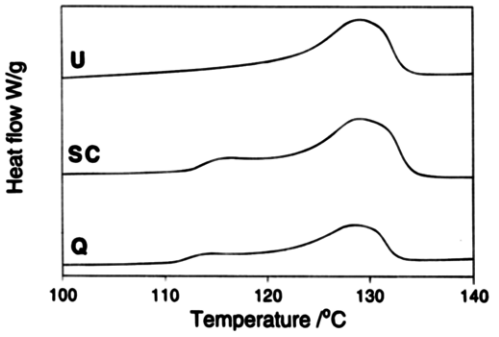

Figure 12. DSC curves showing the melting transition for the untreated (U), slow-cooled (SC), and quenched (Q) LLDPE samples.

in single textured PE, that the CRSS for the martensitic transformation is likely to be of the same order of magnitude as that for chain slip.[40,41] Furthermore, in solution-grown single crystals of PE the activation of the martensitic transformation before chain slip has been observed.[42] Although there is a difference between the structures of the materials used in those experiments and the bulk melt-crystallized samples used in this work, the activation of the martensitic transformation at strains as low as 0.06 need not be too surprising (note that the local strain will be higher than this).

At this point the importance of simultaneous measurement of the SAXS and WAXS patterns becomes apparent, since we have shown (compare ϵ_1 and ϵ_{void} in Table 2) that in the HDPE the martensitic transformation coincides with the onset of cavitation. Following cavitation the chain-folded lamellar structure is deformed into microfibrils.[26] Thus, in bulk HDPE, the martensitic transformation occurred as the structure began to become microfibrillar.

The decrease in intensity of the monoclinic $(\bar{2}01)$ peak which was observed in the annealed HDPE samples drawn at 5.0 mm/min past strains of about 0.3, but not for any of the other samples, cannot easily be explained. Three possible explanations can be proposed, in the knowledge that the monoclinic phase has been shown to be metastable, existing only under stress and below 110 °C.[43] First the loss of constraint due to cavitation may result in some local stress relaxation in these samples, resulting in conversion of some monoclinic material back to the orthorhombic structure. The

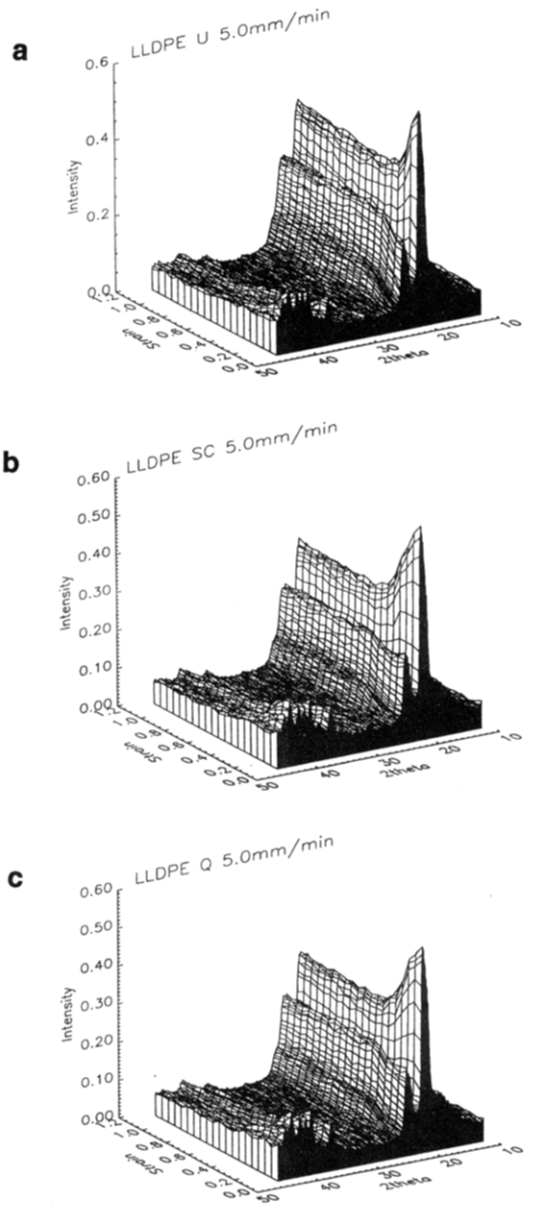

Figure 13. Three-dimensional plot of $I(2\theta)$ vs 2θ vs strain showing the evolution of the wide-angle reflections during drawing for LLDPE drawn at 5.0 mm/min: (a) untreated; (b) slow-cooled; (c) quenched.

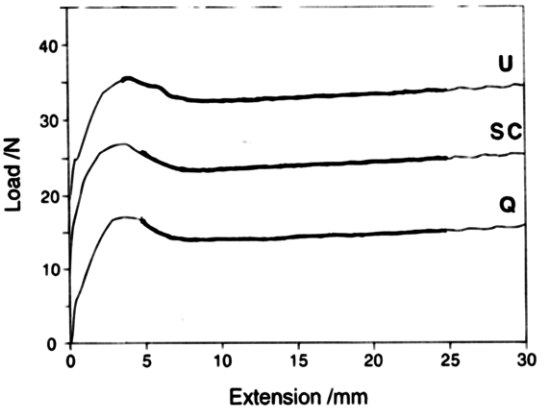

Figure 14. Load–extension curve for the untreated (U), slow-cooled (SC), and quenched (Q) LLDPE samples drawn at 5.0 mm/min.

second explanation is in terms of the melting and recrystallization process proposed by some workers.[27–29] If local heating during deformation allowed tempera-

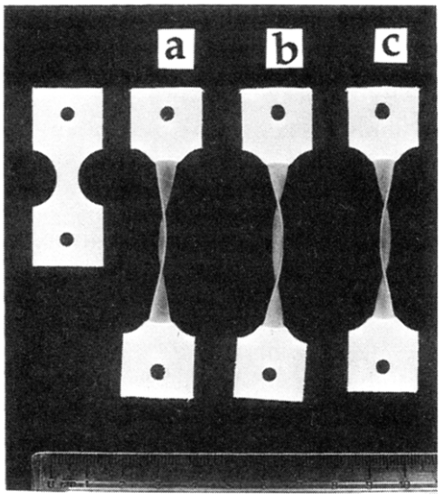

Figure 15. Appearance of the LLDPE samples after drawing and relaxation: (a) untreated; (b) slow-cooled; (c) quenched. The twist in the neck can be clearly seen. An undeformed specimen is also shown.

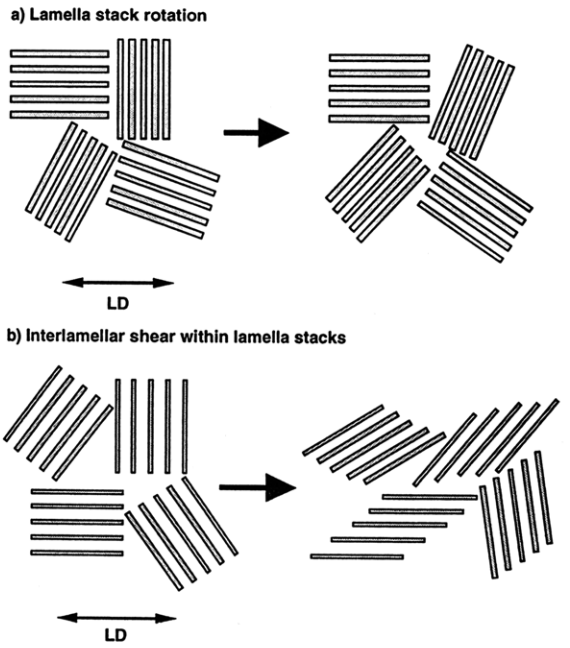

Figure 16. Proposed interlamellar deformation mechanisms operative in the HDPE and LLDPE samples studied.

tures above 110 °C to be reached, then monoclinic material formed at lower strains would become unstable and revert to the orthorhombic form. A third possible explanation is that the loss of monoclinic material is due to disruption by molecular orientation.[44]

The distinguishing factor between the annealed HDPE samples and all of the others is the large amount of cavitation, hence more widespread loss of constraints, occurring in them. However, the samples remain under stress and molecular orientation increases as deformation proceeds. Moreover, cavitation occurs in the amorphous regions whereas the martensitic transformation occurs in the crystalline component. Thus it is uncertain whether sufficient relaxation could occur: the formation of voids might change the stress field sufficiently to allow the required relaxation in the crystallites. An alternative mechanism of relaxation in the crystallite remnants of the fragmented lamellae, in which the monoclinic material is contained, may also be possible if the majority of the deformation of the fibrillar structure occurs in the amorphous component separating the crystallites.

Calculations, according to Peterlin's micronecking model, have shown that adiabatic drawing, in which no heat dissipation occurs to the environment and all the work of drawing is involved in destruction of the lamellae, could lead to high heating effects, reaching maximum temperatures of 110–120 °C. Although these temperatures lie in the temperature regime in which the monoclinic phase is unstable, it has been proposed that they are unlikely to be reached and that there may well be very little temperature increase at all.[26] However, Hendra et al. suggested that local heating is, in fact, sufficient to cause melting and recrystallization.[44] Evidence for melting and recrystallization has also been found in neutron scattering experiments.[27–29] Hendra et al. also suggested the third possibility but discounted it in favor of melting and recrystallization. Faced with these uncertainties, we conclude that the evidence is insufficient to draw definite conclusions and that the reason for the loss of monoclinic material remains uncertain.

4.2. LLDPE. For LLDPE the decrease in long period suggests that the initial deformation mechanism, in the amorphous regions, is interlamellar shear (shown in Figure 16). A similar result was found by Pope and Keller in LDPE.[16] The fact that the long period decreases most at the onset of deformation suggests that the majority of the initial deformation occurs by this mechanism. As expected, further deformation occurs after activation of crystallographic mechanisms, evidenced by the appearance of reflections from the monoclinic phase. However, the continuing decrease of the long period after these reflections appeared shows that mechanisms involving both amorphous and crystalline components coexist during deformation.

From the effect of annealing, i.e., an increase in strain at which the martensitic transformation occurred, it is suggested that crystallographic slip occurs in preference to martensitic transformation. Annealing the LLDPE increased the percentage crystallinity but not the lamellar thickness (see Tables 1 and 3). Thus the annealing dependence of the deformation behavior of LLDPE is due to the increased percentage crystallinity. Increased percentage crystallinity and crystalline perfection might be expected to increase the ease of chain slip by allowing a less hindered translation of chains past each other. Thus in the more perfectly crystalline annealed samples a greater amount of chain slip is possible before the martensitic transformation becomes necessary. It is proposed that this is the reason why the martensitic transformation occurred at higher strains in the slow-cooled and quenched LLDPE.

As observed for the HDPE, further martensitic transformation also ceased to occur in the LLDPE after a certain strain. An explanation for this is that the formation of monoclinic material only occurs for certain orientations of the PE chains relative to the draw direction. This suggestion is supported by previous work on single crystals[25] which has shown that as PE molecules become increasingly aligned, a certain orientation is reached after which no further monoclinic material can be formed. In the LLDPE, as for the HDPE, increasing alignment occurs, but the larger amount of amorphous material allows this to happen without cavitation at the strains reached.

4.3. Comparison of the HDPE and LLDPE. Common to both HDPE and LLDPE was the occurrence

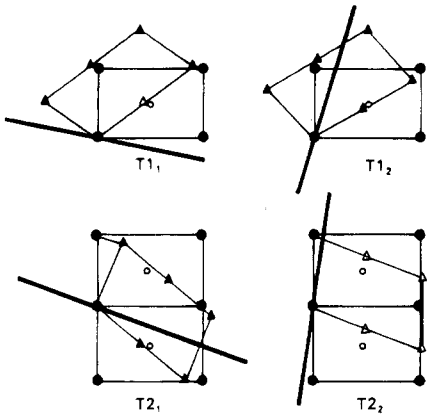

Figure 17. Schematic representation of the four most common modes of martensitic transformation projected on the (001) plane.[24]

of the martensitic transformation at, or near, the yield point. It should be noted that because the load–extension curves were not obtained from the same samples as the X-ray scattering data, further relation of the load–extension curves to the martensitic transformation strain is impossible. The most noticeable feature of the WAXS data for HDPE and LLDPE is the direct correlation between the decrease of the orthorhombic (110) intensity with the increase in intensity of the monoclinic ($\bar{2}01$) intensity, while the orthorhombic (200) intensity remains constant. This implies that the martensitic transformation mode must be one in which the orthorhombic unit cell is sheared such that the (110) planes are destroyed but the orthorhombic (200) planes remain the same as a set of Bragg planes in the monoclinic unit cell. Bevis and Crellin studied the possible transformation modes and reduced them to four principal modes,[24] illustrated in Figure 17, which shows the orientational relationship between the orthorhombic unit cell and the monoclinic unit cell into which it is sheared during deformation. These four modes have been identified as the most likely on the grounds that the active modes will be the ones which require the least transformation shear strain. The transformation shear is $\gamma = 0.201$ for the $T1_1$ and $T1_2$ modes and $\gamma = 0.318$ for modes $T2_1$ and $T2_2$.[5] In single crystals the operative modes have been identified as $T1_1$ and $T2_1$. Only $T1_1$ has been identified in thin melt-crystallized films.[1] By inspection of Figure 17 we propose that the operative mode in the bulk samples used in our experiment was the $T2_2$ mode.

The difference in deformation behavior of the HDPE and LLDPE can be explained by the different lamellar thicknesses and percentage crystallinities. In LLDPE the lamellae are much thinner and more widely separated than in HDPE. There is also more amorphous material due to the branch content, allowing the amorphous component to contribute more to the deformation and interlamellar shear to occur. The higher yield strain, greater physical relaxation of the LLDPE samples used to obtain the load–extension curves, and lack of cavitation in the LLDPE provide further evidence for the larger amount of deformation of the amorphous component in the LLDPE samples. In the HDPE the lamellar stacks will be more rigid because the lamellae are both thicker and closer together, restricting deformation of the interlamellar region within stacks of lamellae. These stacks will only be able to move as a rigid block. Hence limited lamellar stack rotation will occur. Less deformation of the amorphous component will be possible before crystalline deformation mechanisms become active in the HDPE.

5. Conclusions

The use of high-flux synchrotron radiation and fast, position-sensitive, area detectors has allowed the structural changes in PE during deformation on the molecular and supramolecular scales to be followed in real time by means of the simultaneous measurement of the small- and wide-angle X-ray scattering patterns. The relative importance of different deformation mechanisms in different types of PE was shown by using linear low-density and high-density PE's.

A stress-induced martensitic transformation, corresponding to the conversion of orthorhombic to monoclinic material, was detected for both PE's. In HDPE the martensitic transformation occurred during conversion of the lamellar structure to an oriented microfibrillar one. In LLDPE the lamellar structure was also destroyed, although no cavitation occurred. This effect was attributed to the greater freedom of deformation of the amorphous component. The $T2_2$ mode is proposed as the operative martensitic transformation mode in bulk HDPE and LLDPE. In the HDPE it is proposed that lamellar stack rotation occurred. Inhibition of lamellar stack rotation in the annealed, more crystalline, HDPE with thicker lamellae is suggested as an explanation for the activation of the martensitic transformation at lower strains in these samples. In LLDPE the thinner, more widely spaced, lamellae caused interlamellar shear to occur. Increasing the crystallinity of the LLDPE promoted the ease of crystallographic slip mechanisms, leading to higher martensitic transformation strains. The results support the proposition that the stress-induced martensitic transformation occurs after the other deformation mechanisms have become active and that further formation of monoclinic material is unfavored once the molecules have attained a certain orientation. In LLDPE the martensitic transformation is activated at higher strains than in the HDPE because a greater amount of deformation is borne by the amorphous component.

Acknowledgment. The help of the following people is gratefully acknowledged: Dr. Elinor Kerr, of BP Chemicals, Mary Vickers, of the Department of Materials Science and Metallurgy, University of Cambridge, and Pete Bone and Keith Papworth, of the Cavendish Laboratory, University of Cambridge. The financial support of the EPSRC and BP Chemicals is acknowledged.

References and Notes

(1) Bartzcak, Z.; Cohen, R. E.; Argon, A. S. *Macromolecules* **1992**, *25*, 4692.
(2) Bartzcak, Z.; Cohen, R. E.; Argon, A. S. *Macromolecules* **1992**, *25*, 5036.
(3) Bartzcak, Z.; Argon, A. S.; Cohen, R. E. *Polymer* **1994**, *35*, 3427.
(4) Vickers, M. E.; Fischer, U. *Polymer* **1995**, *36*, 2667.
(5) Lin, L.; Argon, A. S. *J. Mater. Sci.* **1994**, *29*, 294.
(6) Bowden, P. B.; Young, R. J. *J. Mater. Sci.* **1974**, *9*, 2034.
(7) Bras, W.; Mant, G. R.; Derbyshire, G. E.; O'Kane, W. J.; Helsby, W. I.; Hall, C. J.; Ryan, A. J. *J. Synchr. Rad.*, in press.
(8) van Aerle, N. A.; Braam, A. W. M. *Colloid Polym. Sci.* **1989**, *267*, 323.
(9) van Aerle, N. A.; Braam, A. W. M. *Makromol. Chem.* **1988**, *189*, 1568.
(10) Wilke, W.; Bratrich, M. J. *J. Appl. Crystallogr.* **1991**, *25*, 645.
(11) Kennedy, M. A.; Peacock, A. J.; Mandelkern, L. *Macromolecules* **1994**, *27*, 5297.

(12) Bassett, D. C.; Hodge, A. M. *Proc. R. Soc. (London)* **1981**, *A377*, 61.
(13) Bassett, D. C.; Hodge, A. M. *Proc. R. Soc. (London)* **1981**, *A377*, 25.
(14) Bassett, D. C.; Hodge, A. M. *Proc. R. Soc. (London)* **1981**, *A377*, 37.
(15) Young, R. J.; Bowden, P. B.; Ritchie, J. M.; Rider, J. G. *J. Mater. Sci.* **1973**, *8*, 23.
(16) Pope, D. P.; Keller, A. *J. Polym. Sci., Polym. Phys. Ed.* **1975**, *13*, 533.
(17) Allan, P.; Crellin, E. B.; Bevis, M. *Philos. Mag.* **1973**, *27*, 127.
(18) Allan, P.; Bevis, M. *Philos. Mag.* **1980**, *41*, 555.
(19) Allan, P.; Bevis, M. *Philos. Mag.* **1977**, *35*, 405.
(20) Hay, I. L.; Keller, A. *J. Polym. Sci.* **1970**, *C30*, 289.
(21) Pierce, R. H., Jr.; Tordella, W. M. D.; Bryant, J. *J. Am. Chem. Soc.* **1952**, *74*, 282.
(22) Tanaka, K.; Seto, T.; Hara, T. *J. Phys. Soc. Jpn.* **1962**, *17*, 873.
(23) Kiho, H.; Peterlin, A.; Geil, P. H. *J. Appl. Phys.* **1964**, *35*, 1599.
(24) Bevis, M.; Crellin, E. B. *Polymer* **1971**, *12*, 666.
(25) Steidl, J.; Pelzbauer, Z. *J. Polym. Sci.* **1972**, *C38*, 345.
(26) Peterlin, A. *J. Mater. Sci.* **1971**, *6*, 490.
(27) Phillips, P. J.; Philipot, R. J. *Polym. Commun.* **1986**, *27*, 307.
(28) Wignall, G. D.; Wu, W. *Polym. Commun.* **1983**, *24*, 354.
(29) Wu, W.; Wignall, G. D.; Mandelkern, L. *Polymer* **1992**, *33*, 4137.
(30) Young, R. J. *Philos. Mag.* **1974**, *30*, 585.
(31) Young, R. J. *Mater. Forum* **1988**, *11*, 210.
(32) Crist, B.; Fischer, C. J.; Howard, P. R. *Macromolecules* **1989**, *22*, 1709.
(33) Zhou, Z.; Lu, X.; Brown, N. *Polymer* **1993**, *34*, 2520.
(34) Hoffman, J. D.; Davis, G. T.; Lauritzen, J. I., Jr. *Treatise on Solid State Chemistry*; Plenum Press: New York, 1976; Vol. 3.
(35) Wunderlich, B. *Macromolecular Physics*; Academic Press: New York, 1973; Vol. 1.
(36) Bras, W.; Derbyshire, G. E.; Ryan, A. J.; Mant, G. R.; Felton, A.; Lewis, R. A.; Hall, C. J.; Greaves, G. N. *Nucl. Instrum. Meth. Phys. Res.* **1993**, *A326*, 587.
(37) Lee, Y. D.; Phillips, P. J.; Lin, J. S. *J. Polym. Sci., Polym. Phys. Ed.* **1991**, *29*, 1235.
(38) Baltà-Calleja, F. J.; Vonk, C. *X-ray Scattering of Polymers*; Elsevier: Amsterdam, 1989.
(39) Bunn, C. W. *Trans. Faraday Soc.* **1939**, *35*, 482.
(40) Young, R. J.; Bowden, P. B. *Philos. Mag.* **1974**, *29*, 1061.
(41) Burnay, S. G.; Aere, M. D. D.; Groves, G. W. *J. Mater. Sci.* **1978**, *13*, 639.
(42) Wu, W.; Argon, A. S.; Turner, A. P. L. *J. Polym. Sci., Polym. Phys. Ed.* **1972**, *10*, 2379.
(43) Kiho, H.; Peterlin, A.; Geil, P. H. *J. Polym. Sci.* **1965**, *B3*, 157.
(44) Hendra, P. J.; Taylor, M. A.; Willis, H. A. *Polymer* **1985**, *26*, 1501.

MA9504072